JOURNAL OF MATERIALS SCIENCE 29 (1994) 987–994

Cobalt intergranular segregation in WC–Co composites

J. VICENS, M. BENJDIR, G. NOUET
Laboratoire d'Etudes et de Recherches sur les Matériaux, URA CNRS no. 1317, ISMRa, Université de CAEN, 6 Boulevard du Maréchal Juin, 14050 Caen Cedex, France
A. DUBON, J.Y. LAVAL
Laboratoire de Physique du Solide, UPR CNRS no. 5, ESPCI, 10 rue Vauquelin, 75232 Paris Cedex 05, France

Interfaces between carbide grains in the tungsten carbide–cobalt composite have been considered. Different techniques, such as transmission electron microscopy and energy dispersive X-ray analysis have been used to characterize the orientation relationship, the nature of the planes and the chemical composition of the grain boundaries.The cobalt concentration at WC–WC grain boundaries was determined by X-ray energy selective analysis in the TEM. Cobalt profiles were performed across low-angle grain boundaries, coincidence and general grain boundaries. Cobalt segregation was found whenever dislocations were imaged in the grain-boundary plane of a low-energy grain boundary. The segregation value was compared with the segregation ratio measured in special grain boundaries characterized by a coincidence site lattice.

1. Introduction

The major constituent in most cemented carbides is a hard and brittle carbide dispersed in a soft and ductile binder phase, each phase is used because of its specific properties: hardness to resist wear, softness to increase toughness. A typical cemented carbide is the composite material tungsten carbide–cobalt (WC–Co). This material is prepared by a liquid-phase sintering process. The cobalt phase acts as the binder phase and the very low interfacial energy between carbide and cobalt phases leads to nearly perfect wetting and to very good adhesion in the solid state [1, 2]. As shown in a recent work [3], the electronic configuration of metals could be a major controlling factor in the thermokinetic reactions that take place during sintering in these materials. On this basis, cobalt appears also to be the most suitable additive/binder in WC–Co. During the sintering process at 1400 °C, the liquid cobalt phase dissolves tungsten carbide crystals to a minor extent. After saturation of the liquid cobalt phase and during specimen cooling, precipitation and growth of WC crystals occur giving rise to the well-characterized microstructure of such composites.

In any polycrystalline material, interfaces and especially carbide–carbide grain boundaries in WC–Co composites play an important role in determining thermomechanical properties. There have been many discussions concerning the continuity of WC crystals, or the existence of continuous cobalt films in intergranular zones and a large number of techniques have been involved: TEM analysis such as lattice imaging [4], high-resolution electron microscopy [5], energy dispersive X-ray analysis [6–8], Fresnel fringe imaging [9] or analytical experiments, namely Auger spectroscopy [10, 11] and atom-probe field-ion microscopy [12, 13]. Moreover the sintering process induces the formation of many WC grain boundaries found close to coincidence orientations which are characterized by a coincidence site lattice (CSL) with a low coincidence index Σ [5, 14, 15]. (The Σ index is defined as the ratio of the CSL volume to the volume of the WC unit cell.) Thus the cobalt segregation amount is expected to be correlated to the crystallographic nature of grain boundaries between WC grains [16, 17].

The aim of the present work was to perform cobalt segregation analyses in various carbide grain boundaries previously characterized by TEM. The cobalt segregation is discussed with respect to crystallographic data.

2. Experimental procedure

WC–Co cemented carbides ("UGICARD") containing 20 wt % Co were prepared by liquid phase sintering at 1400 °C. Cemented carbides based on WC–Co also usually contain small additions of carbide phases such as (Ti,W)C. After sintering these additions form a second phase, the cubic carbide (Ti,W)C (γ phase). Phase intergranular zones were sometimes detected but have not yet been studied. The mean WC grain size was 1 μm. Thin foils were

0022–2461

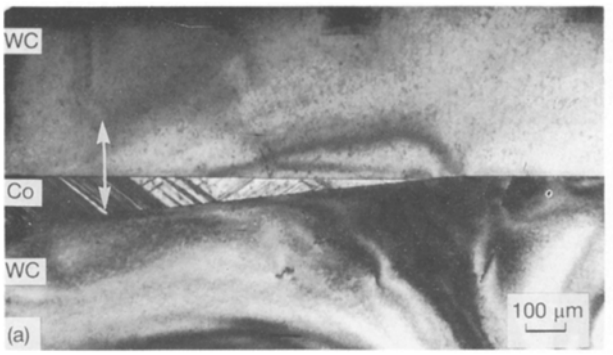

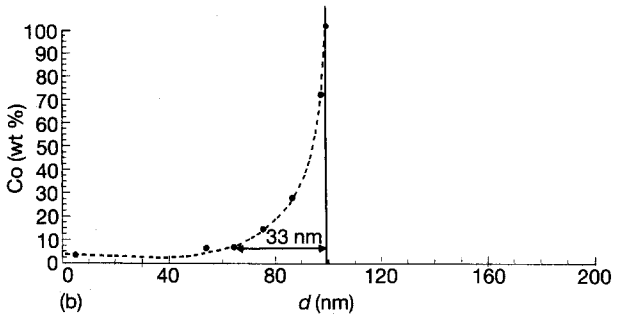

Figure 1 (a) Interphase boundary between a WC crystal and the cobalt phase observed by TEM and (b) the corresponding cobalt profile taken across the WC–Co boundary.

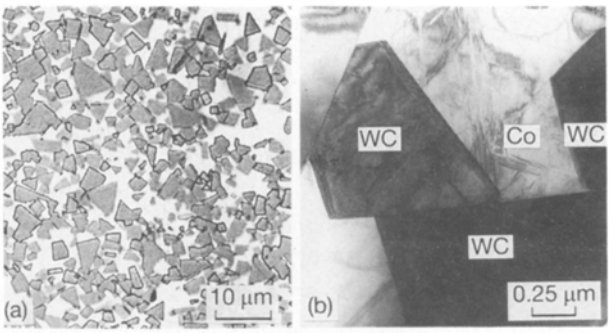

Figure 2 (a) Optical micrograph of a WC–Co sample (20 wt %) with (b) the corresponding transmission electron micrograph.

prepared for TEM studies (Jeol 100 CX) by ion milling (Ar^+, 6 kV). The cobalt concentration in carbide grains and in intergranular zones was measured using X-ray energy selective analyses by considering the L_α-8.425 keV peak for tungsten and the nearby K_α-7.065 keV peak for cobalt. Analysis was performed in the spot mode perpendicular to the grain boundary, orientated parallel to the electron beam. All the cobalt profiles were obtained at the same foil thickness ($\simeq$ 200 nm). This thickness was measured by means of thickness fringes (extinction distance $\xi_{10\bar{1}1}$ = 45 nm). In our experiments, the mean spatial resolution diameter was approximately equal to 30 nm. This value was deduced from the cobalt profile observed at the tungsten carbide–cobalt interphase boundary shown in Fig. 1a and b (arrowed area in Fig. 1a).

3. Results

3. 1. Microstructure and crystallographic data

Optical (Fig. 2a) and transmission electron micrographs (Fig. 2b) illustrate the typical WC–Co microstructure which consists of tungsten carbide crystals (grey) embedded in a cobalt phase (white in Fig. 2a). During the sintering process, tungsten carbide crystals develop well-defined crystallographic facets (Fig. 2b). Furthermore, carbide crystals tend to reach an equilibrium shape, e.g. a triangular prism limited by the basal (0001) plane and three equivalent prismatic $\{10\bar{1}0\}$ planes of the hexagonal carbide structure (a = 0.2906 nm, c = 0.2837 nm) [2]. Typical grain shapes with rectangular or triangular faces can be seen in Fig. 2 exhibiting (0001) crystallographic orientations for triangular crystals. This also suggests that many grain-boundary planes between WC crystals are in well-defined crystallographic orientations because the contacts between prismatic and/or basal planes are favoured.

Geometric descriptions of these carbide grain boundaries were performed by using coincidence models [14]. Theoretical coincidence orientations leading to the formation of a coincidence site lattice (CSL) between the two adjacent crystals were calculated in the hexagonal carbide structure. These results were then compared with experimental orientations found between carbide crystals.

Coincidence orientations were calculated by considering the approximation $c/a = 1$ (instead of the realistic value of 0.976). It was found that many grain boundaries were very close to coincidence orientations with low coincidence index Σ. A high number of these orientations could be described by rotations around the $\langle 10\bar{1}0 \rangle$ or $\langle 11\bar{2}0 \rangle$ crystallographic axes. Fig. 3a illustrated a Σ2 orientation between two carbide crystals observed in the high-resolution electron microscope. The boundary plane $(10\bar{1}0)$ was parallel to the electron beam and the two crystals were rotated by 90° around the $[10\bar{1}0]$ direction. The relative position of the hexagonal cells of the two crystals are described in Fig. 3b. Discontinuities were noted at the boundary plane (arrowed areas in Fig. 3a) consisting in regularly spaced steps. They resulted from the small mismatch between a and c parameters ($41a = 42c$) [5].

The different types of grain boundaries that have been analysed are listed in Table I. These grain boundaries

TABLE I Geometric description of analysed WC grain boundaries

Grain boundary	Σ	Rotation axis	Rotation angle	Deviation from Σ	Grain-boundary plane
1	1	$\langle 11\bar{2}0 \rangle$	3°	–	$\{10\bar{1}0\}_{1,2}$
2	2	$\langle 10\bar{1}0 \rangle$	90°	6°	$\{10\bar{1}0\}_{1,2}$
3	2	$\langle 10\bar{1}0 \rangle$	90°	1°7′	$\{10\bar{1}0\}_{1,2}$
4	5	$\langle 10\bar{1}0 \rangle$	53°13′	1°8′	$\{10\bar{1}0\}_{1,2}$
5	5	$\langle 10\bar{1}0 \rangle$	53°13′	7°	$\{10\bar{1}0\}_{1,2}$
6	43*d*	$\langle 11\bar{2}0 \rangle$	75°18′	1°2′	$\{0001\}_1 \parallel \{30\bar{3}1\}_2$
7	32*b*	$\langle 3\bar{1}\bar{2}0 \rangle$	55°77′	4°7′	$\{10\bar{1}1\}_1$
8	50	$\langle 2\bar{1}\bar{1}3 \rangle$	23°07′	2°7′	$\{10\bar{1}0\}_1$

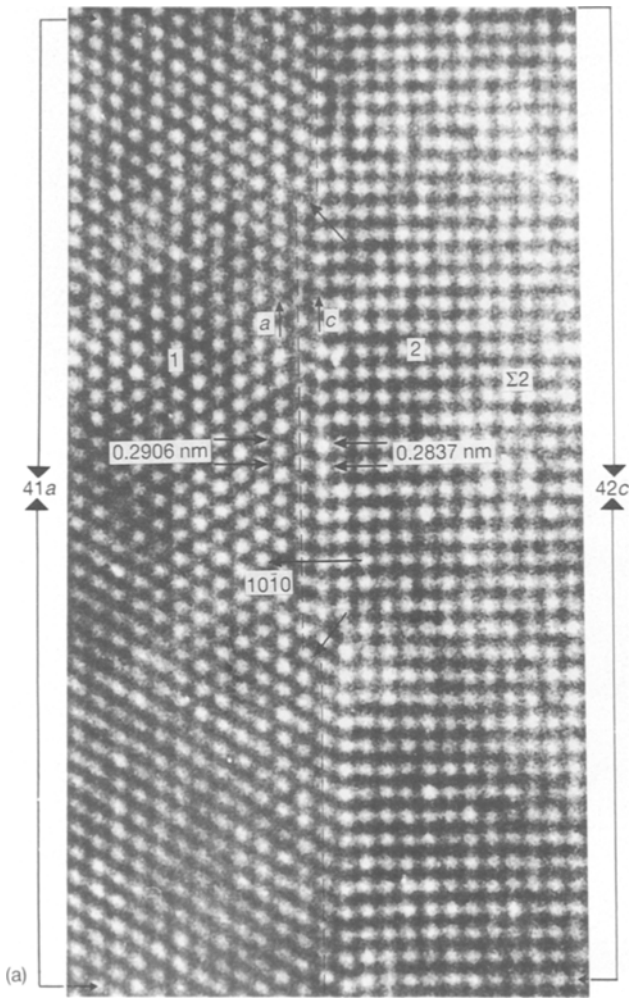

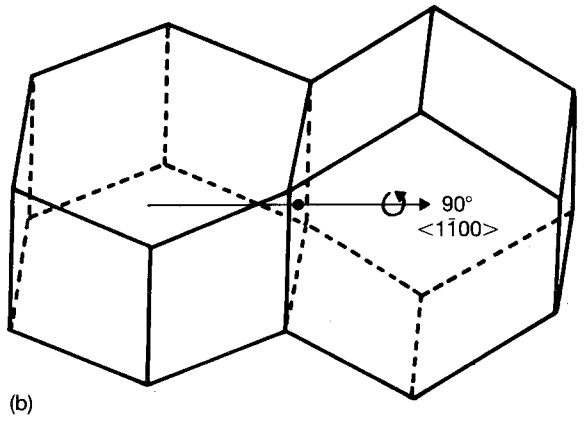

Figure 3 HREM micrograph of a WC–WC grain boundary. (a) The two WC crystals depict a Σ2 crystallographic orientation. (b) Schematic drawing of two hexagonal unit cells rotated by 90° around [1 0 $\bar{1}$ 0].

are defined by the coincidence relationship, Σ, the rotation axis and angle. The deviation from the theoretical coincidence angle is then considered. Finally, the crystallographic nature of the grain-boundary plane is given. Two types of boundaries are revealed, e.g. symmetrical (1–5) and asymmetrical (6–8). Symmetrical grain boundaries parallel to (1 0 $\bar{1}$ 0) prismatic planes were observed with the highest frequency. Example 1 corresponds to a low-angle grain boundary with a tilt character while grain boundaries 2–5 are near coincidence Σ2 and Σ5 with a twist configuration. Grain boundary 6 can be described with a high Σ index as the last two cases. In fact, they are close to general descriptions in terms of CSL. However, grain boundary 6 corresponds to an asymmetrical tilt boundary plane parallel to the (0 0 0 1) basal plane for one crystal only and grain boundary 8 admits again a prismatic plane for one of the crystals.

3.2. X-ray microanalysis

3.2.1. Subgrain boundary

Among the grain boundaries listed in Table I, only one case is seen to be a low-angle grain boundary between two adjacent WC crystals (Fig. 4a). In the orientation shown, the grain-boundary plane $(1\bar{1}00)_{1,2}$ is parallel to the electron beam. The two crystals are slightly misorientated (3°) around the [1 1 $\bar{2}$ 0] common axis (Fig. 4b). This misorientation induces the formation of regular primary dislocations visible in the enlargement (Fig. 4c). Dislocations lie in a wall of $a/3\langle 1\,1\,\bar{2}\,0\rangle$ mixed dislocations seen edge-on. From the crystallography of tungsten carbide it can be deduced that only a component of the Burgers vector of these dislocations gives rise to the tilt rotation of the subgrain boundary [18, 19]. A very limited wetting of the cobalt phase can be observed in area A (Fig. 4a). A cobalt concentration profile has been measured (across the subgrain boundary) in area B (Fig. 4a). This curve (Fig. 4d) reveals the presence of cobalt with a segregation ratio $\simeq 1.6$.

3.2.2. High-angle grain-boundary analyses

3.2.2.1. Special grain boundaries. Four grain boundaries listed in Table I (2–5) have been found close to coincidence orientations: Σ2, (grain boundaries 2 and 3) and Σ5, (grain boundaries 4 and 5). Σ2 is observed very frequently, whereas Σ5 is more scarce. Grain boundaries 2 –5 are illustrated in Figs 5a–8a, respectively. In the orientations shown all the boundary planes are parallel to the electron beam. The corresponding cobalt profiles are displayed in Figs 5b–8b. The Σ2 boundary 2 (Fig. 5) does not exhibit any segregation. The cobalt analysis (Fig. 5b) has been performed across the zone marked A. The Σ2 grain boundary 3 (Fig. 6a) separates two crystals, one of them (grain 2) containing a high density of dislocations. These dislocations interact with a large part of the grain-boundary plane inducing a broadening of the projected image (arrowed zones). These dislocations have an extrinsic character. A segregation ratio of $\simeq 2$ has been found in this case (Fig. 6b).

In the first Σ5 boundary 4 no noticeable segregation was found. TEM did not reveal any dislocation at the boundary (Fig. 7a and b). This has been also verified by tilting the grain-boundary plane with respect to the electron beam. In the second Σ5 grain boundary 5 shown in Fig. 8a and b, a cobalt segregation $\simeq 1.3$ was detected. In such a case, a regular arrangement of dislocations can be seen edge on in the enlargement of the micrograph (Fig. 8a).

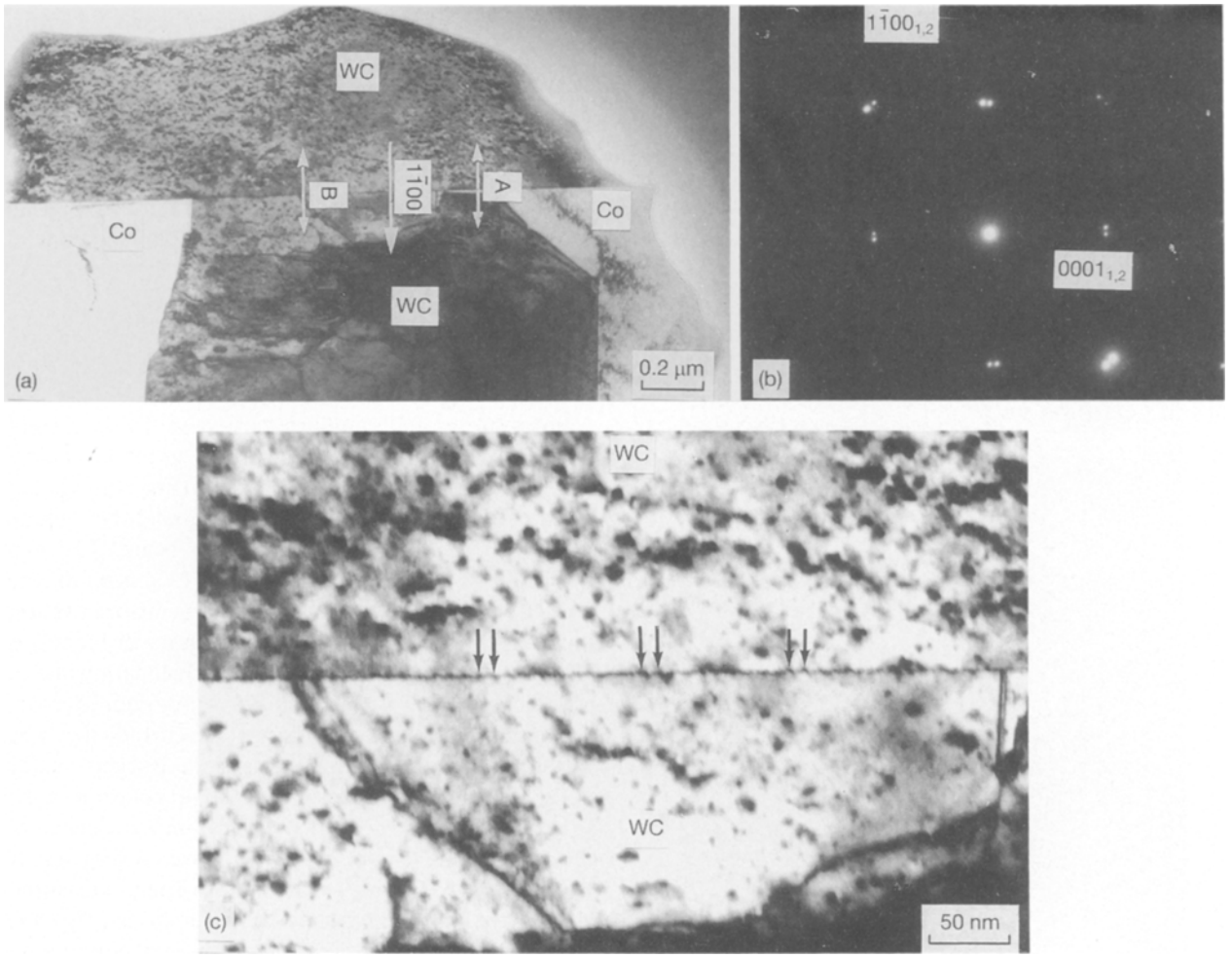

Figure 4 (a) Low-angle grain boundary between two WC crystals with a cobalt film wetting the grain boundary in a very limited part, marked A. The cobalt analysis has been performed across part B. (b) Corresponding diffraction pattern of the subgrain boundary showing the small rotation of the two crystals around the $[1\,1\,\bar{2}\,0]$ axis. (c) Dislocations are imaged in the boundary plane. They are viewed edge-on and some of them have been arrowed on the micrograph. (d) Cobalt segregation profile across the low-angle grain boundary taken in part B.

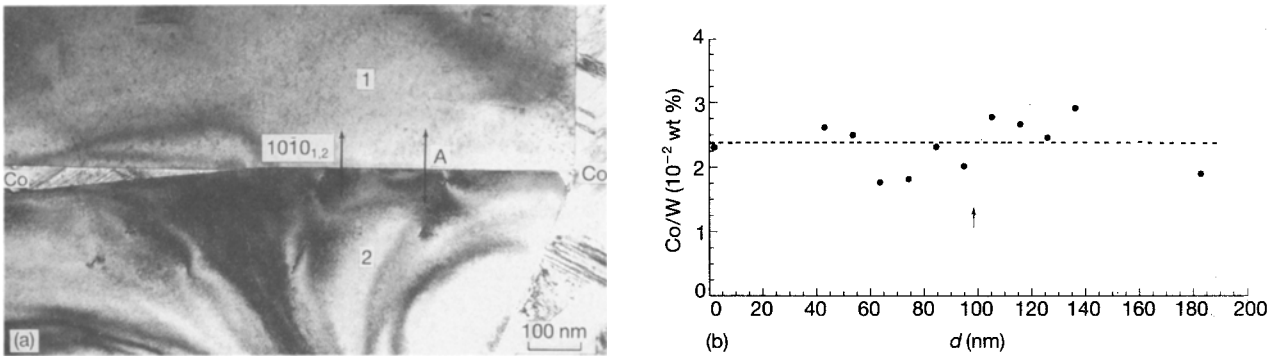

Figure 5 (a) Σ2 grain boundary. A perfect dewetting of the cobalt phase is observed, except in a very small area of the grain boundary. (b) Corresponding cobalt segregation profile across the zone marked A.

3.2.2.2. General grain boundaries. To a first approximation, grain boundaries 6–8 in Table I are labelled as general grain boundaries. The cobalt profiles carried out on grain boundary 6 does not reveal any cobalt enrichment at the interface. However, a slight difference in cobalt amount was observed for the adjacent grains (Fig. 9a and b). For grain boundary 7 illustrated in Fig. 10a, two cobalt profiles were meas-

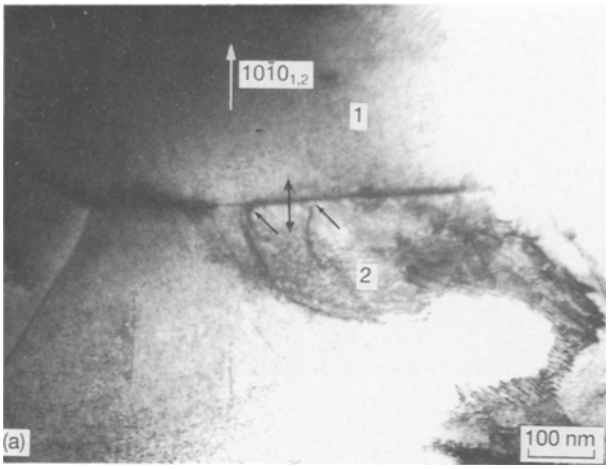

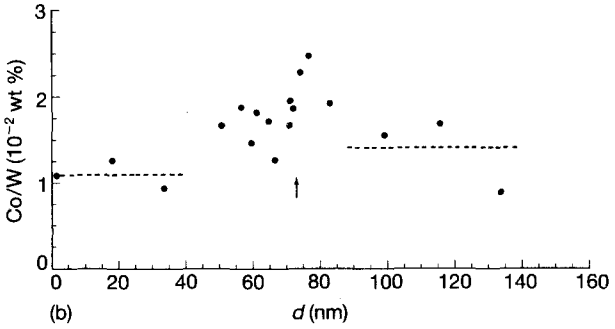

Figure 6 (a) Σ2 grain boundary. Several extrinsic dislocations which have interacted with the boundary plane. Two of them have been arrowed. (b) Cobalt segregation profile.

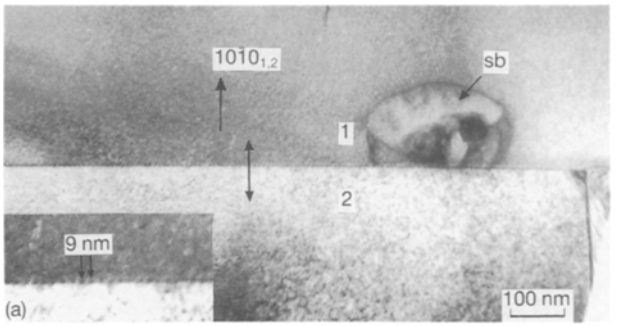

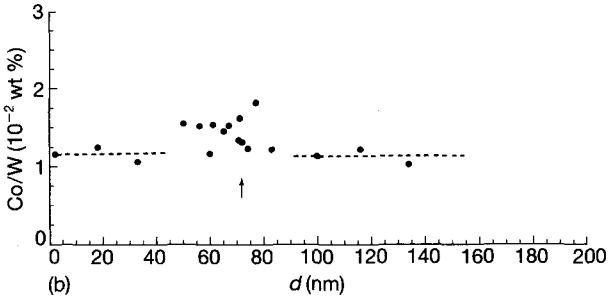

Figure 8 (a) Σ5 grain boundary with a regular array of intrinsic dislocations with the separation distance equal to 9 nm (enlarged part). A subgrain (sb) can be seen in crystal 1. (b) Cobalt concentration profile.

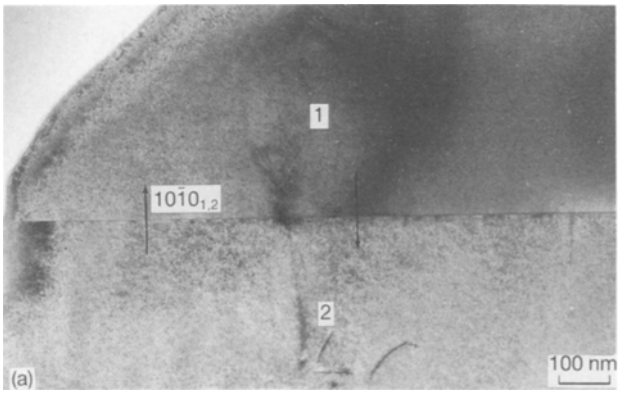

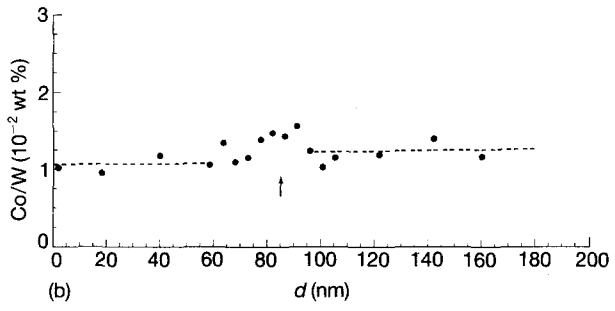

Figure 7 (a) Σ5 grain boundary and (b) its corresponding cobalt concentration profile.

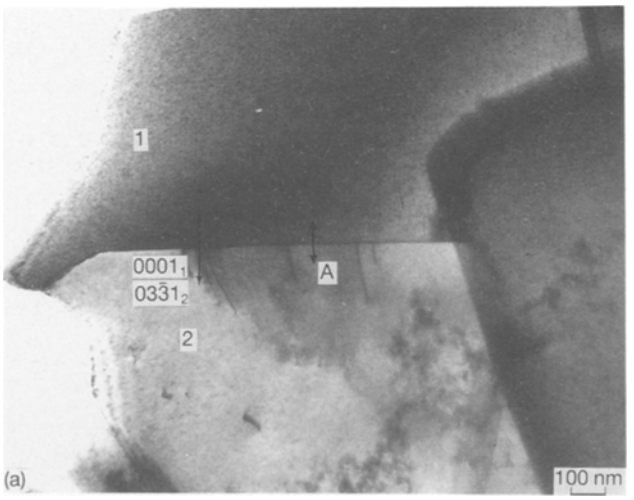

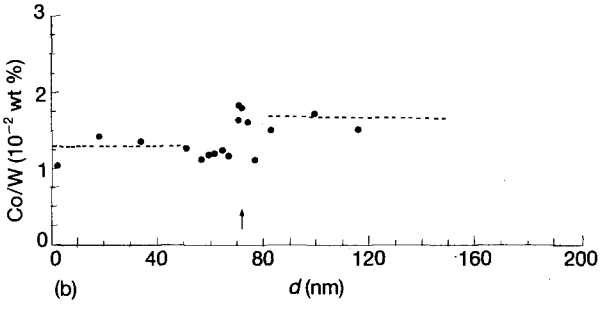

Figure 9 (a) General grain boundary (Σ 43d) and (b) its cobalt microprofile. The profile was taken at A.

ured, one across the vertical part A parallel to $(1\,0\,\bar{1}\,1)$ (Fig. 10b) and the other near the cobalt pocket area B (Fig. 10c). A high cobalt segregation ($\simeq$ 3) is measured across A, whereas the grain boundary is wetted by the cobalt binder across B. Finally, for boundary 8 which corresponds to the highest Σ index, no cobalt segregation was found (Fig. 11a and b).

The cobalt segregation ratios observed in the selec-

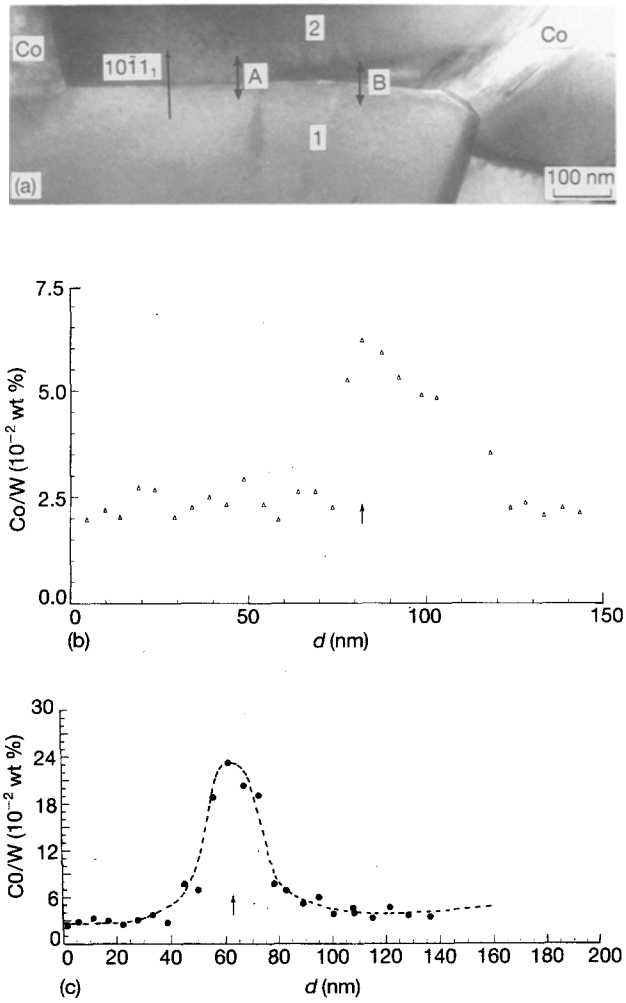

Figure 10 (a) General grain boundary (Σ32*b*). (b) X-ray profile across path A (no visible cobalt film). (c) X-ray profile across path B (5 nm cobalt film).

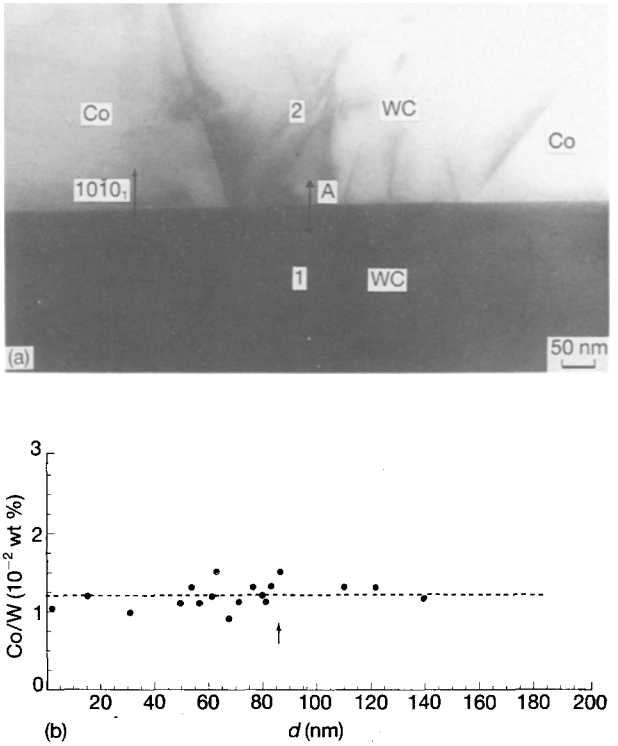

Figure 11 (a) General grain boundary (Σ50) between large WC crystal with a $(10\bar{1}0)$ facet and a small redeposited WC grain. (b) Corresponding cobalt profile across the boundary (part A).

ted grain boundaries are listed in Table II where the possible presence and the character of interfacial dislocations are specified.

4. Discussion

4.1. Intergranular cobalt segregation width

A 30–40 nm mean segregation width equal to our spatial resolution diameter was measured on the cobalt profiles. This was also confirmed when the analysis was performed on thin intergranular cobalt films (> 2 nm) imaged in the TEM at the grain-boundary plane (see, for example, Fig. 10a and b). Therefore, it is not possible in our case to obtain the exact intergranular cobalt segregation width or to ascertain a cobalt gradient at grain boundaries.

In the past these two parameters (segregation gradient and width) had contradictory characteristics reported by different authors. Friederich [8] claimed that cobalt is concentrated in the intergranular areas. His analysis was performed with a small spatial resolution (5 nm). Moreover, cobalt was found to be distributed asymmetrically. The asymmetry of cobalt distribution was assumed to result from grain-boundary migration. The cobalt segregation width extended

TABLE II Intragranular cobalt concentration and segregation ratios in selected WC grain boundaries.

Grain boundary	Σ	Intragranular cobalt concentration, Co/W (wt %)	Intergranular segregation ratios	Micro structure
1	1	2.2	1.6	Primary dislocations
2	2	1	1	
3	2	2.3	1.8	Extrinsic dilocations
4	5	1.1	1	
5	5	1.2	1.3	Intrinsic dislocations
6	43*d*	1.2 ; 1.6	/	
7	32*b*	2.2	3	
8	50	1.2	1	

up to 60 nm, as observed in other materials [20]. This diagnosis is contrary to our results and did not fit the calculation from experiments concerning impurity drag [21, 22]. By contrast, Henjered *et al.* [13] ascertained that cobalt was confined to an intergranular zone (< 2 nm) as measured by atom-probe field-ion microscopy.

By comparing our data with those published by Henjered *et al.*, it can be concluded that the segregation width at carbide boundaries in WC–Co composites has to be less than 40 nm. Furthermore, if Friederich's profiles are also considered, the existence of a cobalt gradient in the vicinity of the grain boundary seems very likely. But from this range of data, it is not yet possible to infer a precise intergranular segregation width and compare this parameter for different types of boundaries.

4.2. Cobalt intragranular concentration

The Co/W ratio for the WC grains deduced from X-ray profiles corresponds to a mean maximum solubility limit of 1.2 wt % Co in a WC grain [7]. This is in good agreement with the value measured in WC–Co by Sharma *et al.* [6] with the same experimental procedure. However, there is a large discrepancy with the data of Friederich [8] and Henjered *et al.* [13]. Friederich [8] found the cobalt content within the grains to be below the detection limit of the X-ray spectrometer (0.2 wt %) whereas Henjered *et al.* [13] gave results indicating no cobalt present, which suggests a solubility of cobalt < 0.003 wt %. Very low cobalt concentration amounts could effectively be measured in our case only if samples were annealed at 1700 °C. At this temperature the cobalt phase is liquid and can partly squeeze out of the WC grains. Moreover, cobalt pockets do still remain at triple junctions. Cobalt profiles across a subgrain (Fig. 12a) and a general grain boundary (Σ37) (Fig. 12b) on the annealed specimen are presented. They indicate that the cobalt solubility is now < 0.2 wt % in WC grains, whereas segregation can still be observed on the subgrain boundary. However WC–Co-base cemented carbide alloys studied by Henjered *et al.* [13] are also commercial grades conventionally manufactured by liquid-phase sintering at about 1400 °C so that the discrepancy reported in cobalt intragranular concentrations remains unexplained.

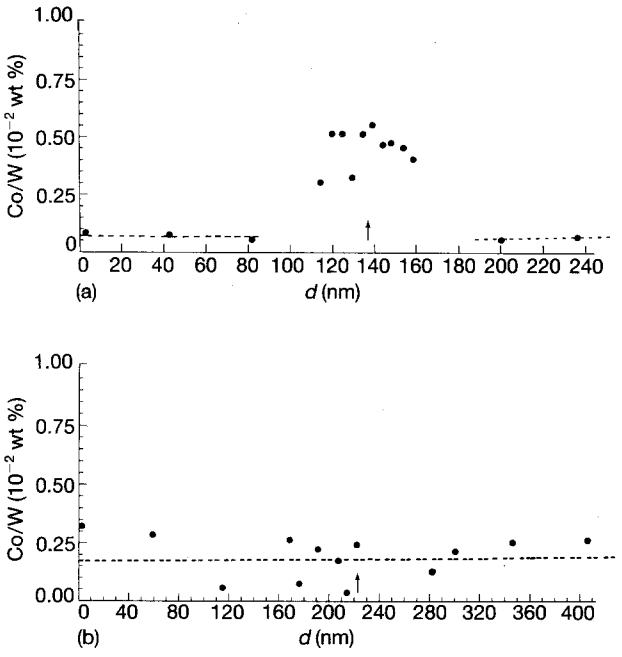

Figure 12 (a) X-ray profile across a low-angle grain boundary in an annealed specimen (1700 °C). (b) X-ray profile measured in a general grain boundary (Σ37) in an annealed specimen (1700 °C).

4.3. Cobalt intergranular segregation

If one assumes that all the cobalt is localized as atomic monolayers at the grain boundary, it is possible to correlate the cobalt concentration with respect to the number of cobalt monolayers. One monolayer is 0.2 nm thick and has the density of h c p cobalt (0.2 nm is approximately the distance between the close packed planes in cobalt). By taking into account the spatial resolution (33 nm), one cobalt monolayer corresponds to 1.5 at % Co or 0.5 wt % Co. Consequently, the number of cobalt monolayers in the analysed grain boundaries ranges from 1–9 monolayers which corresponds to a cobalt film of 0.2–1.8 nm. This latter value has already been proposed by Sharma *et al.* [6] whereas Henjered *et al.* [13] observed only half a monolayer of cobalt. However, we were not able to visualize in the TEM a cobalt intergranular film, even for the general grain boundary (7). This might be explained by the existence of a cobalt gradient at the WC grain boundary.

4.4. Relationships between crystallography and cobalt segregation

In previous studies, only Henjered *et al.* [13] took notice of the crystallography of the grain boundaries. These authors selected two asymmetrical grain boundaries respectively parallel to prismatic $(1\,0\,\bar{1}\,0)$ and $(1\,1\,\bar{2}\,0)$ planes. They concluded that the amount of cobalt did not appear to be dependent on crystallography of the grain boundary.

The results summarized in Table II indicate that there is no clear relationship between the Σ index and the cobalt segregation. Indeed no segregation was found either on low Σ boundaries (Σ2 or Σ5) or high Σ (Σ50). However, by considering the geometry of the boundaries (2, 4 and 8) it is seen that grain boundaries which present a symmetrical character (2 and 4) or which have a prismatic boundary plane for at least one crystal 8 do not exhibit any segregation. Furthermore, an indentical result is obtained on grain boundary 6 which contains the basal plane for one crystal. By contrast, grain boundary which contains a less dense plane $(1\,0\,\bar{1}\,1)$ displays a strong segregation.

Finally, it was shown that subgrain boundary and low Σ boundaries can exhibit a significant segregation ratio. This was ascribed to the presence of different types of dislocations, for example, primary dislocations in a low-angle grain boundary (1), extrinsic

dislocations in a $\Sigma 2$ grain boundary (3) and intrinsic dislocations in a $\Sigma 5$ grain boundary (5). The same phenomena have already been observed in low-angle grain boundaries of different systems. (cobalt, chromium in gold [23], gold in Fe–Au alloys [24]). This is the first time that such data have been observed in this type of material.

5. Conclusion

From our data it can be deduced that the amount of cobalt intergranular segregation depends on the geometry of the grain boundary and the configuration of intergranular dislocations in WC–Co materials. Consideration of coincidence is also relevant, because low Σ grain boundaries very often present a symmetrical grain boundary with dense planes.

Furthermore prismatic planes $(1\,0\,\bar{1}\,0)$ are very often encountered, either in low Σ boundaries ($\Sigma 2$, $\Sigma 5$,...) with a symmetrical configuration or even in high Σ boundaries (such as $\Sigma 50$) with an asymmetrical character. In the latter case, the grain-boundary plane is parallel to the prismatic plane for one crystal. The high frequency of grain boundaries containing a prismatic plane indicates that it is essential to consider the geometry of grain boundaries in order to interpret the mechanical behaviour of such composites. Moreover these data strongly back up the models of the carbide skeleton often used to explain their bulk behaviour.

References

1 H. E. EXNER, *Int. Met. Rev* **4** (1979) 149.
2 H. E. EXNER and H. FISCHMEISTER, *Z. Metallkde* **57** (1966) 187.
3 A. A. OGWU and T. J. DAVIES, *J. Mater. Sci.* **27** (1992) 5382.
4 V. JAYARAM and R. SINCLAIR, *J. Am. Ceram. Soc.* **66** (1983) 137.
5 J. VICENS, E. LAURENT-PINSON, J.L. CHERMANT and G. NOUET, *J. Phys. C5* **19** (1988) 171.
6 N. K. SHARMA, I.D. WARD, H. L. FRASER and W.S. WILLIAMS, *J. Am. Ceram. Soc.* **63** (1980) 194.
7 J. Y. LAVAL, J. VICENS and G. NOUET, *J. Phys. C2* **45** (1984) 695.
8 K. M. FRIEDERICH, *Met. Sci.* **17** (1983) 456.
9 J. N. NESS, W. N. STOBBS and T. F. PAGE, *Phil. Mag, A* **54** (1986) 679.
10 R. K. VISWANADHAM, T. S. SUN, E. F. DRAKE and J. A. PECK, *J. Mater Sci.* **16** (1981) 1029.
11 C. LEA and B. ROEBUCK, *Met. Sci.* **15** (1981) 262.
12 A. HENJERED, M. HELLSING, H. O. ANDRÉN and H. NORDÉN, in " Science of hard materials ", edited by E.A. Almond, C.A. Brookes and R. Warren, (Institute of Physics Engineering Series 75, Bristol, 1986) p. 303.
13 *Idem, Mater. Sci. Technol.* **2** (1986) 847.
14 G. L. BLERIS, G. NOUET, S. HAGEGE and P. DELAVIGNETTE, *Acta Crystallogr.* **A98** (1982) 550.
15 J. VICENS, M. BENJDIR, A. DUBON, J. Y. LAVAL and G. NOUET, in "12 ICXOM", Cracow, Poland, 1989, edited by S. Jasienska and L. T. Maksymowicz, vol. 1 (Institute of Metallurgy, Academy of Mining-Metallurgy, Cracow, Poland, 1989) p. 521.
16 J. VICENS, A. DUBON, J. Y. LAVAL and G. NOUET, in "11 ICXOM', London, Canada, 1987, edited by J. D. Brown and R. H. Packwood, (Ontario, Canada, 1987) p. 356.
17 W. SWIATNICKI, S. LARTIGUE, A. DUBON and J. Y. LAVAL, in "EUREM 92" Grenada, Spain, 10th European Congress on Electron Microscopy, edited by A. Lopez-Galindo and M. I. Rodrigues-Garcia (Secretariado de Publicationes de la Universidad de Granada, Granada, Spain, 1992) p. 749.
18 S. LAY, P. DELAVIGNETTE and J. VICENS, *Phys. Status Solidi a* **90** (1985) 53.
19 S. LAY, F. OSTERSTOCK and J. VICENS, *J. Mater. Sci.* **22** (1987) 1310.
20 L. KARLSSON, H. O. ANDRÉN and H. NORDÉN, *Scripta Metall.* **16** (1982) 297.
21 J. W. CAHN, *Acta Metall* **10** (1962) 789.
22 M. P. SEAH, *J. Phys.* **10** (1980) 1043.
23 J. R. MICHAEL, C. H. LIN and S. L. SASS, *Scripta Metall.* **22** (1988) 1121.
24 A. GREENBERG, Y. KOMEN and C. L. BAUER, *ibid.* **17** (1983) 405.

Received 1 December 1992
and accepted 28 July 1993